BLADE LOAD ANALYSIS ON SWIRL TURBINE RUNNER WITH NONUNIFORM BLADE CASCADE

JAKUB STARECEK, MILOSLAV HALUZA, PAVEL RUDOLF

Brno, University of Technology, Faculty of Mechanical Engineering, Viktor Kaplan Department of Fluid Engineering

DOI: 10.17973/MMSJ.2020_10_2020046

133834@vutbr.cz

Blade load analysis of the turbine blades is generally very crucial for hydraulic machine designs, especially in a case of axial turbines, where the shroud is missing. The torque in this case is transmitted only by the blade pivots or fixed support to hub. Blade loading can be especially significant for off-design operating regimes. Modulation of the excitation frequencies and pressure pulsations is enabled by application of so called nonuniform blade cascades, which leads to different force magnitudes on each of the turbine blades. Therefore, it is necessary to analyse the force acting on each blade by CFD and FEM analysis to adjust thickness of the fixed support or the diameters of the pivots. These analyses are especially important in case of 3D printed plastic runners like in the case of the presented swirl turbine runner.

KEYWORDS

swirl turbine, nonuniform blade cascade, CFD, FEM

1 INTRODUCTION

Most of the unexploited hydroenergy potential in Europe is concentrated in low head locations of small hydropower plants. According to definition small hydro is below 10 MW power output, sometimes further specification is adopted and mini (below 1 MW) and micro (below 100 kW) hydropower sources are classified [Tung 1995, ESHA 2012]. Meaning of "low head" varies considerably, but usually is assigned to heads below 20 meters, whereas very low heads are below 3 meters. There are numerous locations across Europe with sluices or weirs with heads between 1 and 3 meters [ESHA 2012]. Also, throughout the world the potential of low and very low heads remains largely unexploited.

It should also be mentioned that there is yet another place for low head turbines – tidal power plants [Waters 2016]. Although their installations are rather scarce, it is likely that growth, stimulated by green policy subsidies, can be expected in near future.

While Kaplan turbines have been traditionally used for combination of low head and relatively large discharge, their investment costs are rather high due to complex design with adjustable runner blades and guide vanes. Building hydropower plants on low head locations is very sensitive to costs and fast return of investments cannot be achieved with conventional solutions [Narrain 2017].

Swirl turbine, which was developed in 1999 and patented in 2003 by professor Frantisek Pochyly and his team at V. Kaplan Dept. of Fluid Engineering [Patent 2003], with already 3 prototype locations in the Czech Republic presents favourable compromise. It features bulb turbine layout with simple runner with non-adjustable blades and no guide vanes, thus reducing the investment and operating costs [Haluza 2012]. Swirl turbine is very convenient solution for micro- and mini- hydropower plants on locations with very low head. Typical installations are on river weirs, cooling water channels of thermal power plants or wastewater treatment channels. They are also a suitable alternative in case of old hydropower plant refurbishment, where outdated high-specific speed Francis or Kaplan turbines have to be replaced by new machines.

The swirl turbine contains only runner blades and stay vanes, guide vanes are missing. Swirl turbine is working without preswirl of the water at the inlet (the circumferential component of absolute velocity is equal to zero, i.e. $c_{u1} = 0$ m·s^{-1}), as shown in Euler turbine equation [Haluza 2012].

$$g.H.\eta_h = \overbrace{u_1 c_{u1}}^{=0} - u_2 c_{u2} \quad (1)$$

Hence the water at the outlet has negative residual circumferential component ($c_{u2} \neq 0$ m·s^{-1}) as described in equation (2).

$$c_{u2} = -\frac{g.H.\eta_h}{u_2} \quad (2)$$

It is opposite principle than energy transformation in conventional hydraulic turbines (Kaplan or Francis turbine). The model swirl turbine with a uniform blade cascade and six runner blades was designed (runner diameter of D = 194 mm, hub diameter d = 66 mm). The turbine runner is connected to shaft with bearings and gear inside the turbine bulb. Bulb is supported by four stay vanes. The straight pipe intake was used as the water supply. Conical draft tube with rectangular outlet cross section was placed behind the turbine runner. The basic parameters of the particular swirl turbine presented in this paper are design net head H = 3 m, optimal mass flow rate and hydraulic efficiency in BEP (Best Efficiency Point) $Q_m = 0.166$ m^3·s^{-1}, $\eta_h = 75.5$ % respectively, with maximal output power $P_{out} = 3.7$ kW. Four runners with uniform blade cascade (further denoted UR) with different pitch angles (+3°; -3°; -6°; -9°) were designed as additional cases; the plus sign means the runner with higher opening (higher mass flow rates) and the minus means the runners with lower opening (lower mass flow rates), as shown in Fig. 1. The axis of blade rotation in all non-uniformly placed blades on the runner intersects the axis of the runner rotation. The axis of blade rotation is situated at one third of the blade chord at hub surface.

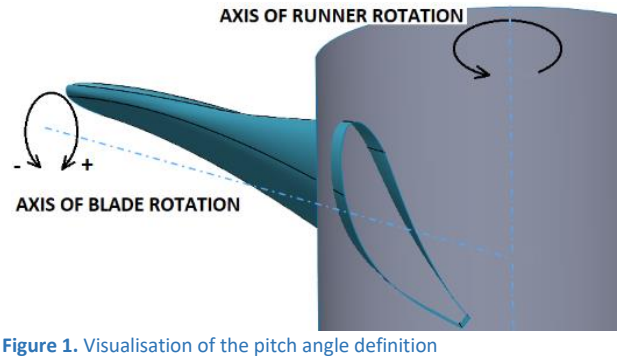

Figure 1. Visualisation of the pitch angle definition

Hydraulic efficiency characteristic curves and blade loadings were investigated and compared for all tested cases. Runners with nonuniform blade cascade (NUR) were designed by combination of blades with different values of pitch angle, every blade set has different position as shown in Fig. 2 (b). Six following combinations of pitch angles: 0° and +3° labelled as (NUR 0°/+3°); 0° and -3° (NUR 0°/-3°); 0° and -6° (NUR 0°/-6°);

0° and -9° (NUR 0°/-9°) were developed. Additionally, next three runners with three different values of pitch angle were designed +3°; 0° and -3° labelled as (NUR +3°/ 0°/-3°) ; 0°, -3° and -6° (NUR 0°/-3°/-6°) and the last -3°, -6° and -9° (NUR -3°/-6°/-9°). The blade layout is shown in Fig 2. (c).

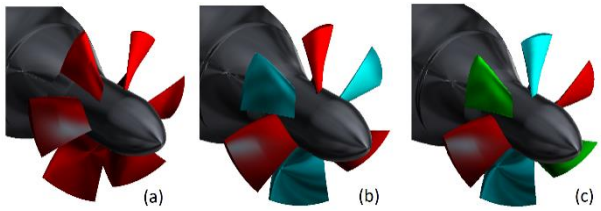

Figure 2. The swirl turbine runners with different layout of blades combination [Starecek 2019-A]

All nonuniform runners were numerically simulated using CFD tools and their characteristic curves were evaluated just like in case of uniform runners. Each blade, which is located in nonuniform runner, is loaded differently. These different loads are caused by velocity shocks on leading edges and different pressure fields on each of the blades. This phenomenon may cause significant changes in loading forces, for example their growth rate or torque transfer.

2 NUMERICAL SIMULATION

Each design was computed by the numerical flow simulation software ANSYS CFX to assess the hydraulic parameters and force magnitudes. The static pressure fields on each blade and rotor parts were obtained from the last timestep. Static pressure data were imported to ANSYS Mechanical for FEM analysis and the static structural analysis was carried out. The equivalent stress and deformation data played a key role for blade thickness and blade radius dimensioning in root section of the blade where it is fixed to the hub.

2.1 *CFD simulation*

Initial turbine runner was designed in ANSYS BladeGen, runners with different pitch angles were created using SolidWorks. All blades have the same design properties, namely the blade length, linear beta angle distribution, NACA profile fourth series shape, 0.3 mm tip gap and blade thicknesses: 12 mm, 9 mm and 6 mm on hub, centre streamline and tip respectively.

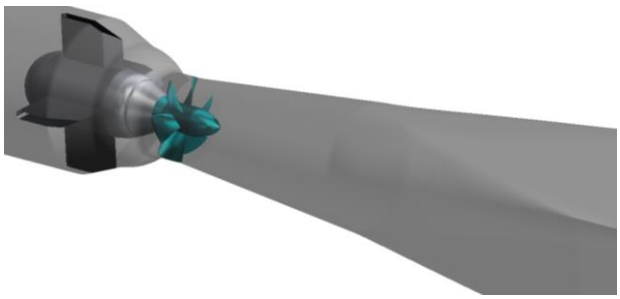

Figure 3. Visualization of the model swirl turbine with stay vanes and conical draft tube

The ANSYS Turbogrid and ICEM CFD were used for generation of the computational mesh for each part. The blade to blade channels in the runner were meshed with fixed periodic boundaries. This approach allowed to combine each blade to runner without having to generate a new computational mesh. All parts had hexahedral computational mesh, only inlet domain contains tetrahedral cells. The volumetric losses in blade tips were taken into account and mesh includes the boundary layer refinements. The computational model of the whole turbine consisted of 2.8 mil. nodes (4.4 mil cells) for uniform case with 0° pitch angle.

	Cells	Nodes
Inlet domain with stay vanes	1 990 499	489 850
Draft tube with outlet domain	982 416	963 200
Blade channel (+3°)	165 008	177 664
Blade channel (0°)	228 080	243 352
Blade channel (-3°)	216 725	232 976
Blade channel (-6°)	261 624	244 757
Blade channel (-9°)	246 056	263 024

Table 1. The overview of mesh parameters for blade channels with different pitch angles

All simulated cases were computed as full transient analysis, where timestep was equal to 2.5° of runner rotation, i.e. for example for n = 1100 min^{-1} timestep Δt = 0.0003788 s was used (all rotating parts are marked as blue colour in Fig.4). Four internal iterations were provided in each time-step. The Shear Stress Transport (SST) turbulence model was used for all simulations. All parts were set as stationary with the exception of the runner. The General grid interface (GGI) was applied between blade channels in the runner (marked by yellow colour in Fig. 4). The transient rotor-stator interface (marked by purple colour in Fig. 4) was applied between rotating runner domain and other stationary domains. The total pressure (P_{tot} = 30 000 Pa) was applied at the inlet (marked by green colour in Fig. 4), to simulate the net head of water (H = 3 m). The static pressure (P_s = 0 Pa) was applied at the outlet (marked by red colour in Fig. 4). The reference pressure (P_{ref} = 1 atm) was set for whole simulation. The no-slip boundary condition with smooth wall definition was applied on all wall faces, so the blade roughness was not include into CFD simulations. (marked as shadow colour in Fig. 4).

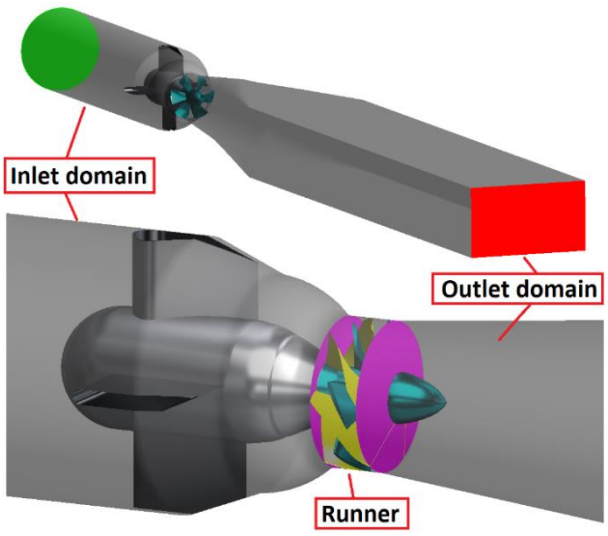

Figure 4. Visualization of boundary conditions and main computational domains

The transient analyses of all ten presented runners were carried out for various RPM, i. e. n_1 = 800 min^{-1}, n_2 = 900 min^{-1}, n_3 = 1000 min^{-1}, n_4 = 1100 min^{-1}, n_5 = 1200 min^{-1}, n_6 = 1300 min^{-1}, n_7 = 1400 min^{-1} and n_8 = 1500 min^{-1}. The unit speed n_{11} [min^{-1}] was defined on basis of the theory of hydraulic similarity to enable comparison between the respective cases.

CFD setup and applied boundary conditions were used according to previous experience at our department. [Pochyly 2019]

$$n_{11} = \frac{n \cdot D}{\sqrt{H}} \quad (3)$$

2.2 FEM analysis

The turbine model contains steel shaft with hexagonal shaped nut (marked as green colour in Fig. 5), which ensures transmission of runner rotation on the shaft. All parts of the runner are made of plastic material: washer, runner and hub cover (marked as red in Fig. 5). All plastic parts are connected by steel recessed bolts. Axial displacement is prevented by steel bolt which goes through the steel hub (marked as green in Fig. 5). The visualization of the construction model, prepared for FEM analysis is in Fig. 5 (the turbine casing and bulb are marked by shadow colour in Fig. 5).

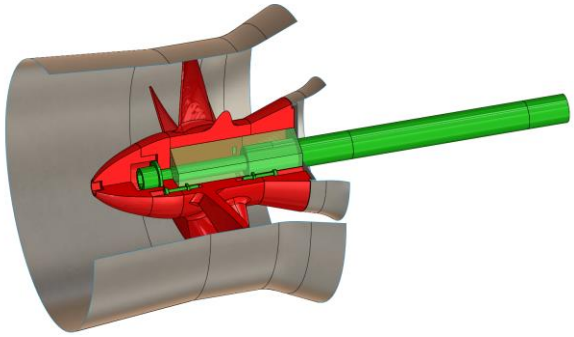

Figure 5. The model of swirl turbine for FEM analyses and following 3D-printing

Red plastic parts are printed by HP Jet Fusion 3D-printing technology from PA 12 (material properties are in Tab 2.). Parts which are not loaded by main forces were made by FDM 3D-printing technology from PETG material. The isotropic material was a prerequisite for FEM analysis. Both materials (construct steel and PA 12) can be considered as linearly elastic. The simulation of blade bending was realized by applying zero displacements in all coordinate directions on the shaft surface which is attached to the hexagonal nut. Whole computational mesh for FEM analysis consisted of ≈ 1.8 mil. linear elements, which represents ≈ 700k nodes.

Material	PA 12 (Red)	Construct steel (Green)
Density [kg·m^{-3}]	1 020	7 800
Young modulus [MPa]	1 800	210 000
Poisson ratio [-]	0.34	0.33

Table 2. Material properties for FEM analysis

3 COMPUTED HYDRAULIC PARAMETERS

Flow rates, torques and pressure differences between inlet and outlet boundaries were obtained from CFD simulations by mass flow rate averaging. IEC 60 193 standard [IEC 60 193] was used for definition of basic hydraulic parameters. Hydraulic efficiency is calculated from equation (4) as ratio between hydraulic output power P_{out} [W] and the hydraulic input power P_{in} [W].

$$\eta_h = \frac{P_{out}}{P_{in}} \quad (4)$$

The hydraulic efficiencies for each operating point were compared using unit speed. Operating range of each design was also investigated. Hydraulic efficiency characteristic curves representing all uniform runners are shown in Fig. 6 and all nonuniform runners characteristics are depicted in Figs. 7 and 8.

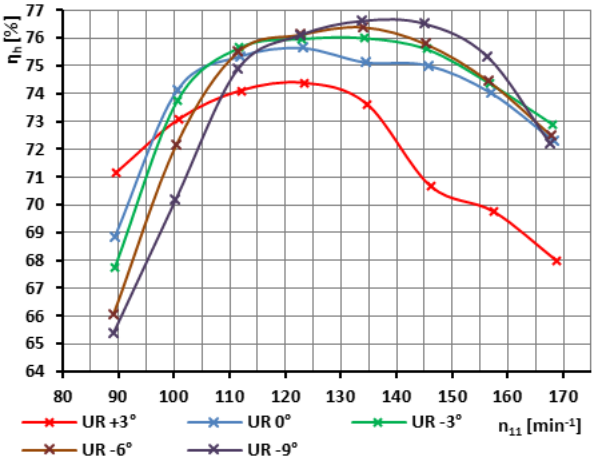

Figure 6. Hydraulic efficiency characteristic curves versus unit speed for uniform runners [Starecek 2019-A]

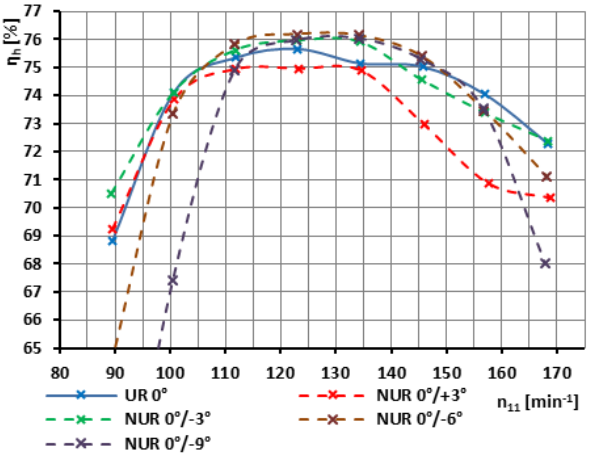

Figure 7. Hydraulic efficiency characteristic curves versus unit speed for nonuniform runners with two sets of blades [Starecek 2019-A]

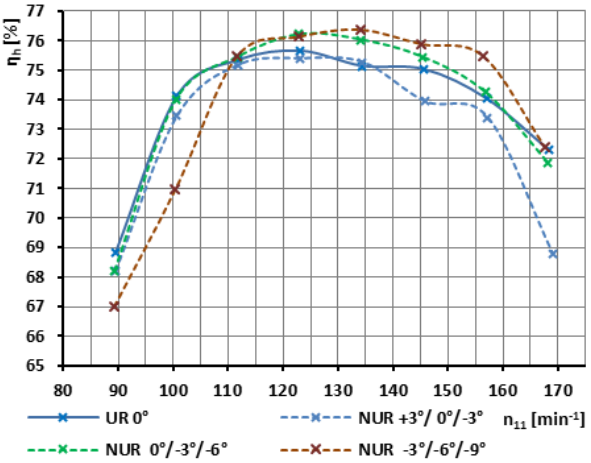

Figure 8. Hydraulic efficiency characteristic curves versus unit speed for nonuniform runners with three sets of blades

Turbine runners for low net head are less affected by nonuniform blade cascades than the higher head ones. By using three blade sets in one runner the influence of nonuniformity grows. The operating range starts to expand and the hydraulic efficiency increases. However, nonuniform runners are source of relatively higher blade loading.

4 BLADE LOADING AND STRUCTURAL ANALYSIS

Blade loadings were evaluated from the CFD simulation by force averaging of the five runner revolutions. Force fluctuations, which are caused by the interaction of the stay vanes and the runner blades are observed. This phenomenon is called rotor-stator interaction (RSI) and the force fluctuations are increasing with decreasing distance between rotor and stator parts. This interaction causes the excitation frequencies and force fluctuations in the turbine. These excitation frequencies can be modulated by applying different position of the leading or trailing edges [Starecek 2019-B]. The force fluctuations were observed during computation, but were not really significant, due to the large distance between stay vanes and runner blades (the force fluctuation was less than 2 % of absolute value in each monitored point for uniform runners and less than 1.3 % of absolute value in each monitored point for nonuniform runners). The force monitors were set on each blade separately to observe differences in blade loading. Mean force values were calculated from obtained data. Blade load figures contain force values for different unit speeds.

4.1 *Forces on runners with uniform blades*

Force acting on all uniform turbine runners rises with decreasing speed (or unit speed n_{11}), which is typical for hydraulic turbines. It is possible to find some exceptions related to off-design regime caused by velocity field changes or separating flow in draft tube, but generally it has increasing tendency. The highest values are related to non-rotating runner (maximal torque on the shaft), on the opposite the lowest values are related to no-load operation (maximal unit speed, i.e. torque is equal to zero). The behaviour of force loading in operating range corresponds to the theoretical assumptions as shown in Fig. 9. Drops in case UR -9° and UR -6° for $n_{11} \approx 100$ min^{-1} are caused by moderate change of angle of attack and pressure distribution on suction and pressure side of the blade. These drops are shifted to lower unit speed in case of -3° and 0° pitch angle.

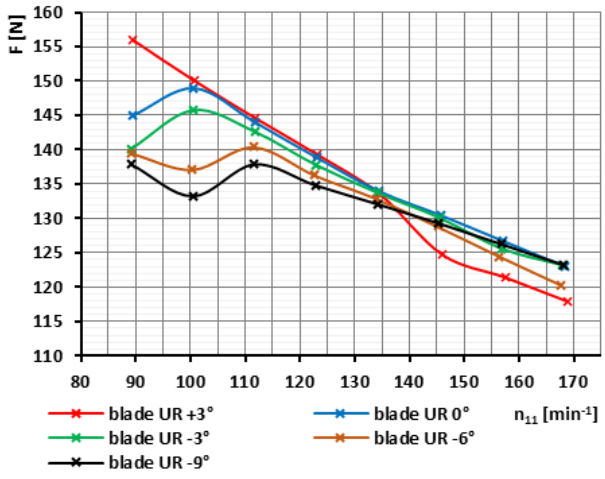

Figure 9. Comparison of blade loading for all uniform cases. [Starecek 2019-A]

The force curves increase with different slope, but force magnitudes close to the best efficiency point are very similar (n_{11} = 123 min^{-1} - 134 min^{-1}). This phenomenon is changed by using nonuniform runner where each blade is loaded by different pressure, resulting in different force magnitudes.

4.2 *Forces on runners with two sets of blades*

The force magnitudes are rapidly offset, even for very small differences in pitch angle, for example 0° and +3° (NUR 0°/+3°) in Fig. 10 or 0° and -3° (NUR 0°/-3°) in Fig. 11.

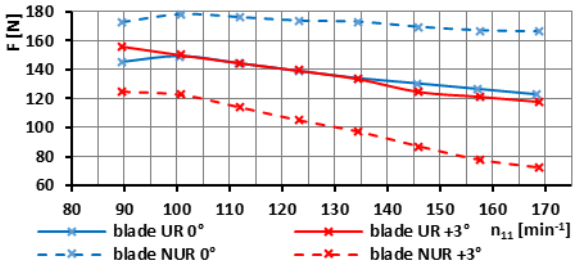

Figure 10. Comparison of blade loading for blades with 3° pitch angle difference (NUR 0°/+3°)

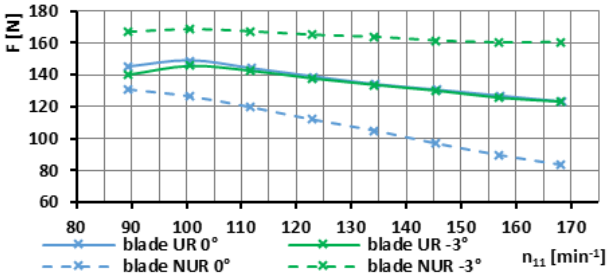

Figure 11. Comparison of blade loading for blades with 3° pitch angle difference (NUR 0°/-3°)

Generally, the leading edge of the blade with lower pitch angle (i.e. lower flow rate) is slightly shifted in terms of axial direction compared with the blade with higher pitch angle (i.e. higher flow rate). The water at the runner inlet is affected by blade set with higher pitch angle and adapts to it. Shifted blades (blades with lower pitch angle) operate with velocity shock on the leading edge. Hence the difference in pressure distribution on the pressure and suction side of the blade increases. This pressure difference caused by velocity shock on blade leading edges, can be visualized by static pressure. Absolute static pressure field for nonuniform runner with 3° pitch angle difference (NUR 0°/-3°) is illustrated in Fig. 12.

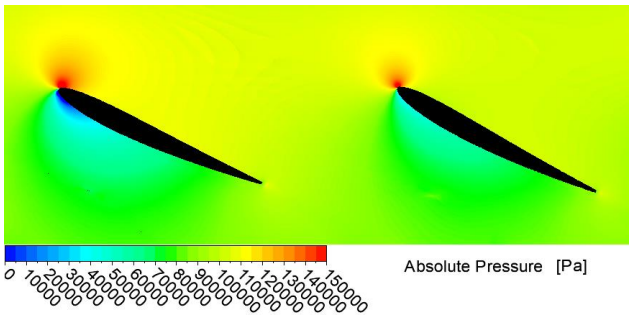

Figure 12. Pressure distribution in blade channel (90% of channel height) n_{11} = 123 min^{-1} (NUR 0°/-3°)

While the pressure difference is increasing, the force magnitudes are also increasing. The blade load difference is proportional to growing pitch angle difference. It is caused by gradual increase of shock on the blade leading edges with lower pitch angle. An accompanying phenomenon is a change in the shape of the blade load characteristic. Part of the blade load characteristic (NUR 0°/-6°) with the unit speed much higher than the best efficiency point (n_{11} > 145 min^{-1}) is constant (force equal to about F = 200 N). On the left side of the curve (n_{11} < 123 min^{-1}), the force magnitudes start decreasing with

decreasing unit speed. This behaviour is totally opposite compared to the uniform blade cascades. The shock on the leading edge on blade in alignment grows, and the blade starts acting as a blockage in the blade channel (represented by brown dashed curve in Fig. 13). This blockage slows down the water flow inside the main blade channel and the static pressure increases. Pressure distribution on the blades with lower pitch angle is affected by static pressure change and the pressure on suction side rises. Forces on the blades with lower pitch angle (higher mass flow rates) are decreasing with lower pressure differences between pressure and suction side, as shown in Fig. 13 (the blades with lower pitch angle are marked by blue colour).

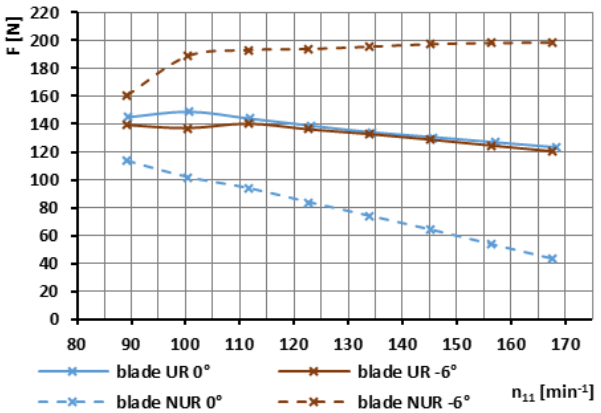

Figure 13. Comparison of blade loading for blades with 6° pitch angle difference (NUR 0°/-6°)

The last case which was tested had significant pitch angle difference between blades 0° and -9° (NUR 0°/-9°). This blade set does not fulfil its function except the best efficiency point. Massive flow separation behind the blades with lower pitch angle was the main problem for runners with relatively big differences in pitch angles, as shown in Fig. 14.

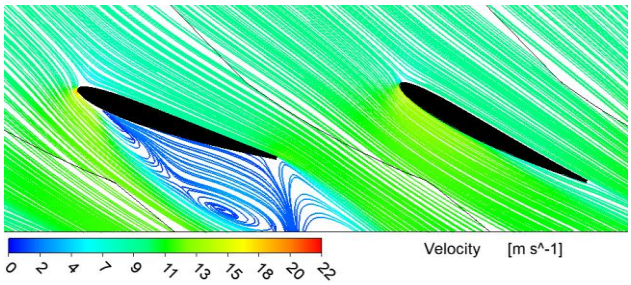

Figure 14. Velocity streamlines in blade channel (90% of channel height) n_{11} = 90 min^{-1} (NUR 0°/-9°)

Force magnitudes were rather apart and blade load characteristic for blade with lower pitch angle is decreasing in whole operating range with decreasing unit speed. The velocity field adapts to a set of blades with higher pitch angle resulting in shockless entry of the flow on these blades. The blades form a blockage and totally lose their proper function due to significant shock on the leading edge (as shown in Fig. 16). and forming of the separation around the blade. As in the previous case, the pressure in the blade channel increased and blades with lower pitch angle are affected. For example, for higher unit speed (n_{11} > 150 min^{-1}), the force magnitudes on lead blade are close to zero (the torque is not transmitted).

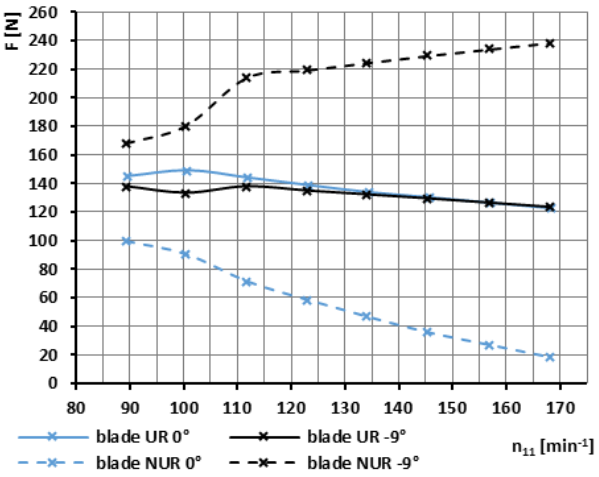

Figure 15. Comparison of blade loading for blades with 9° pitch angle difference (NUR 0°/-9°)

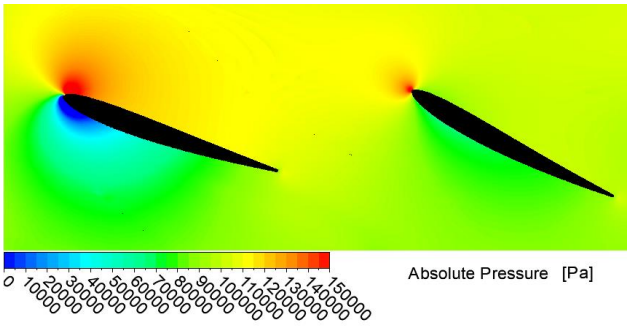

Figure 16. Pressure distribution in blade channel (90% of channel height) n_{11} = 123 min^{-1} (NUR 0°/-9°)

4.3 *Forces on runners with three sets of blades*

Three nonuniform runners with three sets of blades were computed. By using three sets of blades, the force shifting was partially reduced. Blade loading on two blade sets (with the highest pitch angles) increased over the reference case with uniform blades in one runner. On the other hand, blade loading on blade sets with smallest pitch angle significantly dropped. As in previous cases with significant differences in pitch angle, the blades with higher pitch angle affect velocity field close to the runner inlet. Blades in alignment start to act as a blockage in blade channel. The pressure distribution on the blades with higher pitch angle was changed and the forces rapidly decreased.

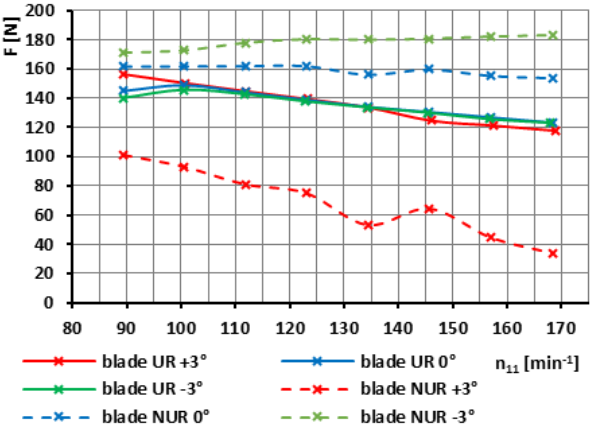

Figure 17. Comparison of blade loading for blades with 3° and 6° pitch angle difference (NUR +3°/ 0°/-3°)

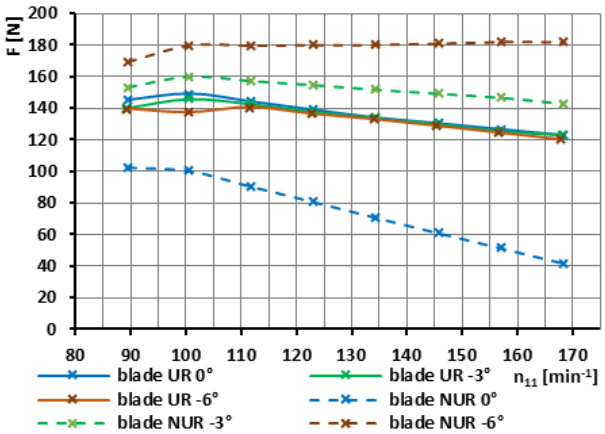

Figure 18. Comparison of blade loading for blades with 3° and 6° pitch angle difference (NUR 0°/-3°/-6°)

Force magnitudes reach their highest values in cases with three sets of blades and can be considered as constant, with changing unit speed. The highest force magnitudes are expected for the best efficiency point.

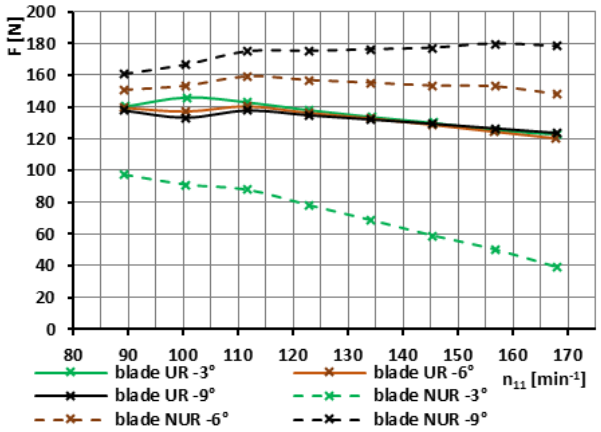

Figure 19. Comparison of blade loading for blades with 3° and 6° pitch angle difference (NUR -3°/-6°/-9°)

	+3°	0°	-3°	-6°	-9°
UR	139.4 100%	138.9 100%	137.8 100%	136.2 100%	134.8 100%
NUR 0°/+3°	105.1 75%	173.4 124%			
NUR 0°/-3°		112 81%	165.2 120%		
NUR 0°/-6°		83.8 62%		193.9 142%	
NUR 0°/-9°		46.6 35%			224.4 166%
NUR +3°/ 0°/-3°	75 54%	162 117%	180 131%		
NUR 0°/-3°/-6°		80.8 58%	180.1 131%	154.6 114%	
NUR -3°/-6°/-9°			78 57%	156.7 115%	175.3 129%

Table 3. Comparison of forces [N] acting on all tested cases for n_{11} = 123 min^{-1}

4.4 *Structural analysis*

The runners with 0° pitch angle (UR 0°), -6° pitch angle (UR -6°) and nonuniform runner with 0° and -6° pitch angle (NUR 0°/-6°) were chosen for testing in hydraulic laboratory. The structural analyses were carried out for these three cases. Each runner design was examined in three operating points, which were defined by unit speed (n_{11} = 100 min^{-1}; n_{11} = 123 min^{-1}; n_{11} = 156 min^{-1}) Maximal deflection and equivalent stress were evaluated. It was necessary to make a structural analysis for the case with 0° and -6° (NUR 0°/-6°), because the force action on the -6° blade was very high (over 142 % higher than for reference uniform case). The uniform cases were also tested by FEM analysis. It is important to keep in mind that blades with different pitch angles have different strength. It is caused by different blade position in the hub.

	n_{11} = 100 (min^{-1})	n_{11} = 123 (min^{-1})	n_{11} = 156 (min^{-1})
UR 0°	0.98 mm 9.5·10^6 Pa	0.97 mm 9.1·10^6 Pa	0.96 mm 8.3·10^6 Pa
UR -6°	0.94 mm 9.7·10^6 Pa	0.94 mm 9.7·10^6 Pa	0.91 mm 9.5·10^6 Pa
NUR 0°/-6°	0.71 mm 1.24 mm 1.39·10^7 Pa	0.68 mm 1.28 mm 1.4·10^7 Pa	0.51 mm 1.35 mm 1.42·10^7 Pa

Table 4. Maximal deformation and maximal stress for chosen tested cases: n_{11} = 100 min^{-1}, n_{11} = 123 min^{-1}, n_{11} = 156 min^{-1}

The maximal deflection of the blades, which is located at the outer radius of the blades is less than 1 mm for uniform cases and 1.24 – 1.35 mm for blades with -6° of pitch angle in nonuniform case (NUR 0°/-6°) (Fig. 20). The blades with 0° pitch angle are least affected (Fig. 21).

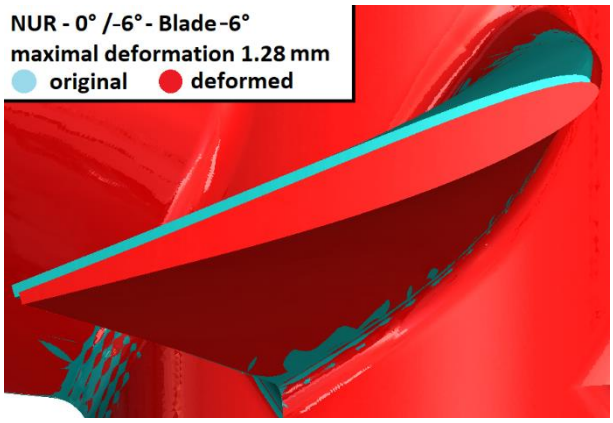

Figure 20. Visualization of maximal blade deformation compared with original undeformed blade: case with non-uniform runner (NUR 0°/-6°, n_{11}=123 min^{-1})

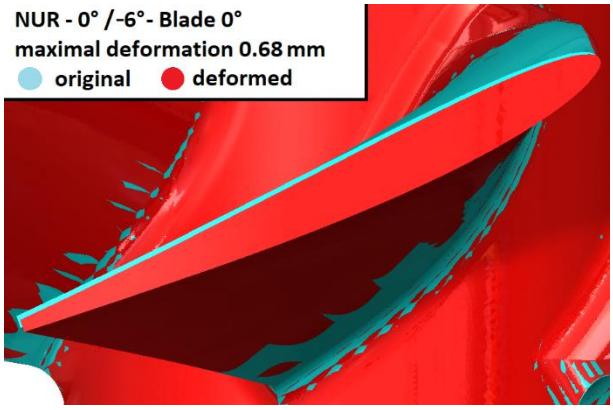

Figure 21. Visualization of maximal blade deformation compared with original undeformed blade: case with nonuniform runner (NUR 0°/-6°, n_{11}=123 min^{-1})

The maximal value of equivalent stress was found to be around $\sigma_{EQV} = 8.3 - 14$ MPa. These maximal values of equivalent stress are located at fixed support, which connects the blade and hub, i.e. at blade root. Since the yield strength of material PA 12 is $\sigma_K = 103.6$ MPa, the corresponding safety factor is higher than ten for uniform cases and seven for nonuniform case. In terms of strength the blades are durable, but it is necessary to accept small deflection and bending. Second CFD analysis of deformed blade shape may be carried out for precise estimation of hydraulic parameters However from previous experience their change is known to be negligible.

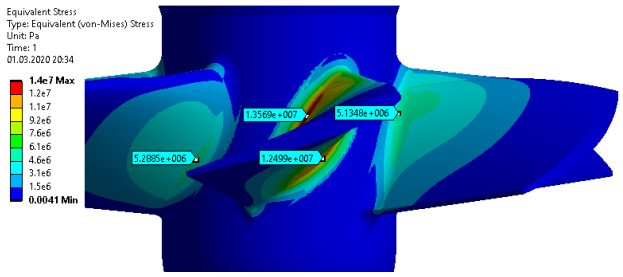

Figure 22. Visualization of maximal stress at fixed support in case with nonuniform runner (NUR 0°/-6°, n_{11}=123 min^{-1})

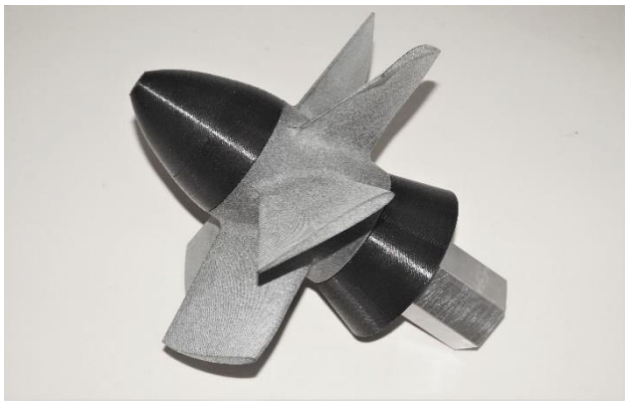

Figure 23. The runner with 0° pitch angle (UR 0°) printed by HP jet fusion technology. Black parts are made by FDM technology. Inside the turbine there is hexagon shape nut with bolt. Presented model is prepared for surface finish and measuring

This runner will be installed to the current existing turbine chamber which is identic as CFD model. The dimension of tip gap can be slightly modified. Turbine is a part of closed hydraulic circuit, which include hydrodynamic pump with frequency converter to ensure flow rates and required net head. The output parameters will be measured by induction flowmeter, dynamometer and pressure gauges at the turbine inlet and behind the draft tube.

5 CONCLUSIONS

Non-uniform blade cascades of hydraulic turbines modulate excitation frequencies and influence the operating range. However, this approach may cause problems with excessive blade loading on some blades inside runner, especially in case of contemporary hydraulic machines where blades are designed as thin as possible to achieve high hydraulic efficiency. Turbine runners or pump impellers without shroud are more sensitive and prone to deformation. The high amount of presented numerical calculations in this paper results in following main conclusions:

- The small pitch angle difference may stabilize the hydraulic parameters (hydraulic efficiency, pressure pulsation or draft tube back flows). The change in velocity shock on leading edges by using nonuniform blade cascades (even with a small pitch angle difference (NUR 0°/-3°)) always occurs.
- In case of higher pitch angle differences one set of blades can perform poorly and behaves as blockage in blade channel. Flow separation was observed for some regimes when using nonuniform runners with relatively large pitch angle differences (NUR 0°/-9°)
- Nonuniform runners with more than 6° difference in blade pitch angle cause change in the shape of blade load characteristics and force loadings are constant for different unit speeds. Blade loadings have the opposite slope of growth within the operating range in some cases (NUR 0°/-9°). This phenomenon is quite different from conventional hydraulic turbine runners.
- The blade loading change (shift of the forces) was observed for all non-uniform cases. Blade loading change is proportional to the pitch angle difference. Nonuniform cascades must be evaluated and well adjusted for using in hydraulic turbines.

The turbine runners manufactured by 3D printing technology may have lower bending stiffness, therefore it is important to analyse blade loading for critical operating regimes. Undesired large deformations may cause change in hydraulic parameters or model destruction in the worst case. Therefore it is important to perform structural analysis prior manufacturing and consider the maximum blade deformation.

Acknowledgments

The research has been supported by project "Computer Simulations for Effective Low-Emission Energy" funded as project No. CZ.02.1.01/0.0/0.0/16_026/0008392 by Operational Programme Research, Development and Education, Priority axis 1: Strengthening capacity for high-quality research

REFERENCES

[Bednar 2013] Bednar, J. Turbiny: (male vodni elektrarny). Ceskovice: Marcela Bednarova, 2013. ISBN-978-80-905437-0-6 (in Czech)

[Narrain 2017] Narrain, A.G.P.: Low Head Hydropower for Local Energy Solutions, CRC Press (2017)

[Vesely 2009] Vesely, J., Pochyly, F. Obrovsky, J. and Mikulasek J. A New Concept of Hydraulic Design of Water Turbine Runners. International Journal of Fluid Machinery and systems. Turbomachinery Society of Japan, Korean Fluid Machinery Association, Chinese Society of Engineering Thermophysics, IAHR, 383-391 (2009)

[Tung 1995] Tung, T.T.P., Bennett, K.J.: Small Scale Hydro Activities of IEA Hydropower Programme. Hydropower and Dams (1995)

[ESHA 2012] Small Hydropower Roadmap: Condensed Research Data for EU-27 (2012)

[ESHA 2012] Waters, S., Aggidis, G.: Tidal range technologies and state of the art in review. Renewable and Sustainable Energy Reviews, Vol 59, pp. 514-529 (2016)

[Haluza 2012] Haluza, M., Pochyly, F. and Rudolf, P. The swirl turbine. IOP Conference series: Earth and Enviromental Science, 2012, 15, DOI: 10.1088/1755-1315/15/4/042034

[Starecek 2019-A] Starecek, J., Cupr, P. Volkov, A., Druzhinin, A. and Haluza, M. Influence of pitch angle on parameters of swirl turbine with uniform and non-uniform blade cascades. International Conference Experimental Fluid Mechanics, November 2019, pp 459 – 466.

[Starecek 2019-B] Starecek, J., Cupr, P. and Haluza, M. Design of high-specific speed turbine with non-uniform blade cascade. EPJ Web of Conferences, 2019, 7, ISSN 2100-014X, DOI: 10.1051/epjconf/201921302078.

[Pochyly 2019] Pochyly, F., Rudolf, P., Stefan, D., Moravec, P., Stejskal, J., and Skotak, A. Design of a pump-turbine using a quasi-potential flow approach, mathematical optimization and CFD. IOP Conference series: Earth and Enviromental Science, 2019, 240, DOI: 10.1088/1755-1315/240/7/072043

[Patent 2003] Pochyly, F., Haluza, M., Rudolf, P., Sob, F.: Swirl turbine, Czech patent No 292197 (2003)

[IEC 60 193] International Standard IEC 60 193: Hydraulic pumps, storage pumps and pump-turbines – Model acceptance tests. International Electrical Commission. Genf. 1999

CONTACTS:

doc. Ing. Pavel Rudolf, Ph.D.
Brno University of Technology, Faculty of Mechanical Engineering
Viktor Kaplan Department of Fluid Engineering
Technická 2896, 616 69 Brno
rudolf@fme.vutbr.cz